

Intertidal beach profile estimation from reflected wave measurements

Rafael Almar^{a,*}, Chris Blenkinsopp^b, Luis Pedro Almeida^c, Erwin W.J. Bergsma^a, Patricio A. Catalan^{d,g,h}, Rodrigo Cienfuegos^{e,g}, Nguyen Trung Viet^f

^a LEGOS, Toulouse, France

^b Water, Environment and Infrastructure Resilience Research Unit, Dpt of Architecture and Civil Eng., University of Bath, UK

^c Instituto de Oceanografía, Universidad Federal do Rio Grande (IO-FURG), Rio Grande, Brazil

^d Departamento de Obras Civiles, Universidad Técnica Federico Santa María, Valparaíso, Chile

^e Dpto de Ingeniería Hidráulica y Ambiental, Escuela de Ingeniería, Pontificia Universidad Católica de Chile, Santiago, Chile

^f Thuy Loi University, Hanoi, Viet Nam

^g Centro de Investigación para la Gestión Integrada del Riesgo de Desastres (CIGIDEN), Conicyt/Fondap/15110017, Santiago de, Chile

^h CCTVal-Centro Científico Tecnológico de Valparaíso, Valparaíso 2390123, Chile

ARTICLE INFO

Keywords:

Nearshore
Reflection
Cut-off frequency
Runup
Beach slope
Wave spectrum

ABSTRACT

The intertidal beach profile provides coastal engineers and managers with a good indication of the current state of a sandy coastline, however regular beach profile measurements are time consuming and expensive to obtain using conventional surveying methods. The potential to reconstruct the intertidal beach profile from measurements of reflected waves is tested here using three field datasets covering a different range of hydro-morphological conditions from dissipative, to reflective. The swash is found to behave as a low-pass filter on reflected waves, with a cut-off frequency that primarily depends on the swash slope. An agreement is found between video-derived swash spectrum saturation tail and the shortest reflected waves, computed from deep water directional wave measurements. By integrating this swash slope over a tidal cycle, the shape of the intertidal beach profile can be reconstructed. Our results clearly show the potential of such method to estimate complex intertidal beach profile, such as double-slope beaches.

1. Introduction

Measurements of beach morphology using traditional methodologies are expensive and time-consuming to obtain. Existing techniques to remotely estimate the intertidal beach profile are based on terrestrial video imagery (e.g. Aarninkhof et al., 2003; Almar et al., 2012; Didier et al., 2017) and Lidar (Blenkinsopp et al., 2010; Phillips et al., 2019) or a combination of both (Andriolo et al., 2018). As such, the ability to estimate the intertidal beach profile based on off-the-coast wave measurements would be a valuable alternative solution which is explored in the present work. Linking wave reflection to the equilibrium beach profile (e.g. Anthony, 1998; Bernabeu et al., 2003; Ludka et al., 2015) is not new. For example, the pioneering studies of Iribarren and Nogales (1949) and Miche (1951) based on laboratory experiments linked incoming waves with surf zone slope, hence vertical acceleration versus gravity, summarized by the surf-similarity number ξ (Battjes, 1974):

$$\xi = \frac{\tan\alpha}{\sqrt{\frac{H}{L}}} \quad (1)$$

where α is the surf zone slope, and H and L the offshore wave height and wavelength respectively, assuming monochromatic waves and a planar slope. Numerous field observations show that this predictor does not work well for irregular waves and complex bathymetry such as two-slope beaches (Mizuguchi, 1984; Elgar et al., 1994; Miles and Russell, 2004). Studies such as Sutherland and O'Donoghue (1998) successfully link wave reflection to the ratio between inclined wall length and shallow water wavelength for the case of an impermeable sloping seawall. Considering an inclined structure, Taira and Nagata (1968) and Suhayda (1974) demonstrate the role played by the swash slope alone in controlling reflection, which is not accounted for when estimating reflection from ξ , though it is noted that their analysis is not valid for natural beaches.

Regarding the spectral signature of reflected waves, significant research effort has been devoted to investigating the link between ξ and the saturation of short waves due to depth-induced breaking (Sallenger and Holman, 1985; Raubenheimer et al., 1996; Baldock and Holmes, 1999; Guedes et al., 2013). In a recent review, Hughes et al. (2014) suggest that wind- and swell-waves (with period $T < 20$ s) are

* Corresponding author.

E-mail address: rafael.almar@ird.fr (R. Almar).

commonly saturated and dissipate (Hughes and Fowler, 1995; Hughes and Mosseley, 2007; Holland et al., 2001), particularly on flattest beaches while the saturation of longer infragravity waves ($T > 20$ s) is less common (Bowen, 1977; Ruessink et al., 1998). Despite this, recent observations have shown that saturation can extend to the infragravity band (Ruggiero and Holman, 2004; Senechal et al., 2011) and infragravity waves can be dissipated through breaking (Van Dongeren et al., 2007; de Bakker et al., 2014; Bertin et al., 2018). Observations at very steep beaches show reflection even in the gravity band (Almar et al., 2014a; 2018a). In the swash zone, several authors (Huntley et al., 1977; Guza and Thornton, 1982; Ruessink et al., 1998) describe a swash spectra saturation roll-off around f^3 (with f the frequency) based on theoretical analysis and observation. This obviously reflects surf-zone wave transformation but is also thought to result from swash-swash interactions that limit the growth of runup with offshore waves (Baldock and Holmes, 1999; Brocchini and Baldock, 2008). The link between the saturation tail of swash, beach slope, and reflected waves has not yet been clearly established, in particular for incoming broadband spectra at complex beaches (e.g. different surf and swash slopes).

This paper provides insights on how the intertidal beach profile can be estimated from the reflected wave spectrum. In Section 2, datasets at three distinct natural beaches covering a range of conditions from dissipative to highly reflective are presented. In Section 3, the relationship between swash spectrum saturation and reflection cut-off frequency, and the related link between the cut-off frequency and the swash slope is investigated. A new method based on these results is applied to estimate daily intertidal beach profiles from offshore wave measurements. Some concluding remarks are provided in Section 4.

2. Data and methods

2.1. Field data

The data used in this paper were collected during three experiments undertaken in 2012–2013 at contrasting field sites (Fig. 1). A dissipative beach experiment was conducted at Mataquito, Chile, from November 28th to December 14th, 2012 (Cienfuegos et al., 2014; Almar et al., 2014b). Mataquito is a medium grain-sized ($D_{50} = 0.2$ mm), alongshore uniform, barred beach with a micro-tidal range and a wave climate dominated by swell waves (annual mean significant wave height, $H_s \sim 2.4$ m, peak period $T_p \sim 12$ s, predominantly from the SW direction). An intermediate beach experiment was conducted at Nha Trang, Vietnam from December 3rd to 10th, 2013 during winter monsoon moderate-energy swell waves (Lefebvre et al., 2014). Nha Trang is an intermediate reflective, medium grain-sized ($D_{50} = 0.3$ mm), alongshore uniform low tide terrace beach with a micro-tidal range and a low to moderate energy wind-wave dominated climate (annual mean, $H_s < 1$ m, $T_p < 5$ s, E). A reflective beach experiment was conducted at Grand Popo, Benin, from February 17th to 28th, 2013. Grand Popo is a reflective, medium to coarse grain-sized ($D_{50} = 0.6$ mm), alongshore uniform, low-tide terraced beach with a micro-tidal range and a wave climate dominated by swell waves (annual mean, $H_s \sim 1.4$ m, $T_p \sim 9.4$ s, SW; Laibi et al., 2014; Almar et al., 2014b).

During the three experiments, significant wave height H_s was moderate (0.9 m–1.5 m) with the tide ranging between 1.1 and 1.8 m. Upper shoreface slope was 0.06, 0.13, and 0.15 at Mataquito, Nha Trang and Grand Popo respectively. Iribarren number ξ ranged from 0.8 at Mataquito, the most dissipative beach, to 2.3 at the most reflective, Grand Popo.

Swash slope is computed daily from differential GPS topographic surveys and tidal levels. Offshore waves (Fig. 1) are estimated from hourly directional wave measurements using an Acoustic Doppler Current Profiler (ADCP) located in a water depth of approximately 10 m at all sites. Incoming and outgoing wave heights were separated from the directional energy density (representing the variance

associated with the defined frequency band and the variation of the incidence angle from the shore-normal direction, see Almar et al., 2014c), following the method described by Sheremet et al. (2002) and Almar et al. (2014c), integrating from the lower to upper cut-off frequency within the gravity-infragravity band (0.02 Hz–0.5 Hz). Swash monitoring using shore-based video was undertaken at 2 Hz during daylight hours at the three experiment sites (Almar et al., 2017, 2018a). Time series of pixel intensity were sampled along a cross-shore line (Holland and Holman, 1993), to create timesteps in order to measure swash runup spectra (Fig. 1) using the method described in Almar et al. (2017). Rectification of images from pixels into real world coordinates was accomplished by direct linear transformation using DGPS ground control points (Holland et al., 2013) after a correction of the radial lens distortion (Heikkila and Silven, 1997). Although varying somewhat throughout the field of view, the pixel footprint was less than 0.1 m in the cross-shore direction over the swash zone.

3. Results and discussion

3.1. Swash saturation and reflected spectrum

The horizontal runup spectra in the lower panels of Fig. 1 show a saturation at higher frequencies ($f > 0.1$ Hz). The tail of saturation extends into the infragravity band ($f < 0.05$ Hz) for the dissipative beach of Mataquito whereas the entire swell-band is unsaturated for the highly reflective beach of Grand Popo. Following the method described in Ruessink et al. (1998), the highest unsaturated frequency (tail of the f^{-3} roll-off) is extracted from hourly spectra and termed the swash cut-off frequency fc_{swash} . This definition is found to be sensitive to the shape of the spectrum, in particular when multiple peaks are observed, but it generally offers a reasonable estimate. While reflected waves propagate offshore and de-shoal, the value of fc is rather constant. With the aim of linking swash saturation with offshore reflected waves, $fc_{offshore}$ is also computed from offshore wave directional spectra (Fig. 1, upper and mid panels), and defined as the highest frequency for which the ratio of outgoing over incoming wave energy is greater than 0.25. Fig. 2 shows that a good fit ($r^2 = 0.68$, significant at 95% level) is obtained between fc computed from swash and offshore waves with only a minor bias (0.93).

Hourly $fc_{offshore}$ is more closely linked to the swash slope α than to ξ computed using α , with correlation coefficients of 0.71 and 0.46, respectively. Confirming the observations of Hughes et al. (2014), this indicates that $fc_{offshore}$ primarily depends on the swash slope α and is rather independent to incoming waves that are also included in ξ . Fig. 3 shows that fc increases with α , with a linear least square best fit giving $fc_{offshore} \sim 0.56\alpha$. Average $fc_{offshore}$ values in the infragravity range 0.02 Hz ($T_c = 39$ s) are observed for the low gradient Mataquito beach ($\alpha = 0.05$) and in the gravity range 0.07 Hz ($T_c = 14$ s) at the steep Grand Popo beach ($\alpha = 0.15$).

On dissipative beaches, rather dominated by surf zone processes, reflection can be appropriately scaled up using deep water parameters (Guza and Thornton, 1982; Díaz-Sánchez et al., 2013). A reflection indicator based on swash processes is less accurate, as swash processes may not be the main control factor, or noise in reflection data is important in relation to the signal itself (Guedes et al., 2011). The reflection coefficient of wave energy is variable within and outside the surf zone, as described by Baquerizo et al. (1997). In contrast, the cut-off frequency of reflected waves is less affected by a complex submerged morphology (Davies, 1982; Mei, 1985) and the transformation of waves (Yu and Mei, 2000) and therefore more conservative. Nevertheless, waves may undergo partial reflection on the shore, followed by re-reflections (Miche, 1951; Elgar et al., 1994, 2003), with wave transformation including frequency transfers that inherently weaken the link between swash dynamics and offshore waves. The dispersion on Figs. 2 and 3 can also be partly attributed to noise from directional wave measurements in coastal waters. The ADCP may have difficulty

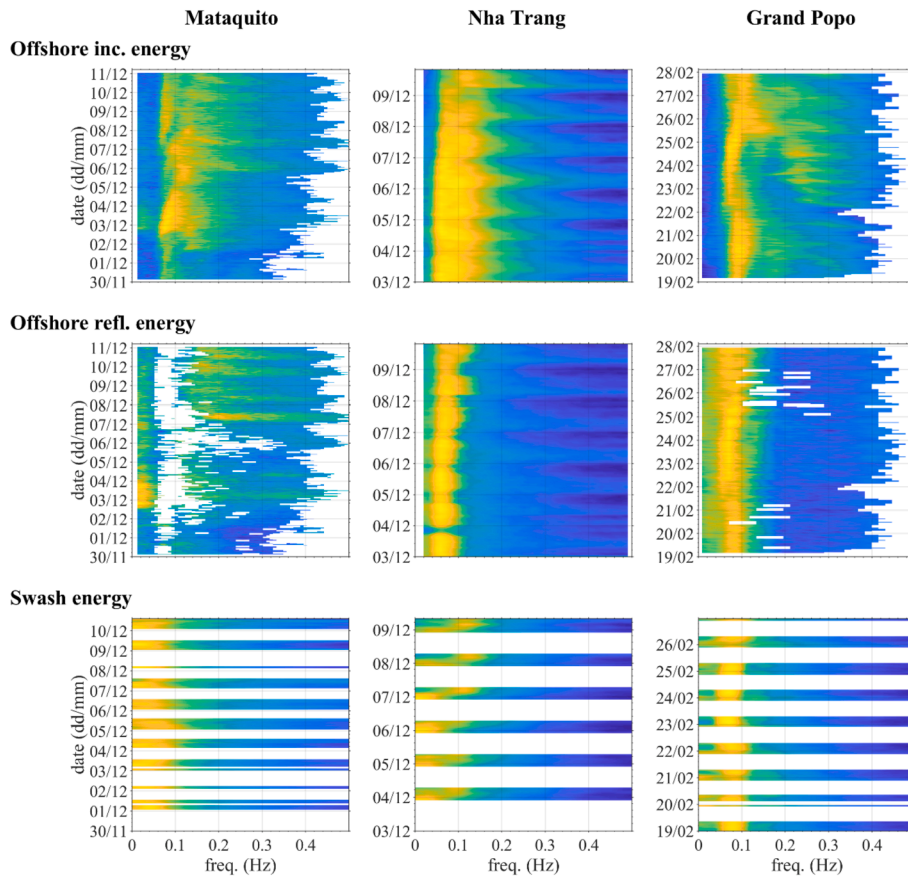


Fig. 1. Incoming and reflected wave spectra at the ADCP (~10 m depth) in upper and mid panels respectively. Swash spectra from video (during daylight hours) are shown in lower panels. All spectra are normalized.

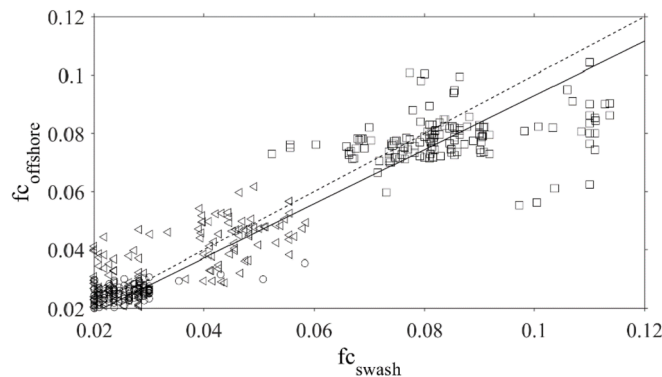


Fig. 2. Hourly cut-off frequency from offshore wave measurements ($fc_{offshore}$) at Grand Popo (squares), Nha Trang (triangles) and Mataquito (circles) as a function of cut-off frequency computed from swash spectra (fc_{swash}). Solid line stands for linear best fit ($fc_{offshore} = 0.93 fc_{swash}$, $r^2 = 0.68$, significant at 95% level) while dashed line is 1:1.

capturing the shortest waves in relatively deep waters. Noise can also result from the notoriously difficult detection of the swash from video imagery (Voudoukas, 2014). Although the Radon Transform method (Almar et al., 2017) based on motion (i. e. flow) detection is expected to be better suited when studying swash shape rather than colour contrast used in pioneering studies of Holland and Holman (1993) and Holland et al. (2001, 2013), deriving swash spectrum and its saturation tail from video remains a challenge.

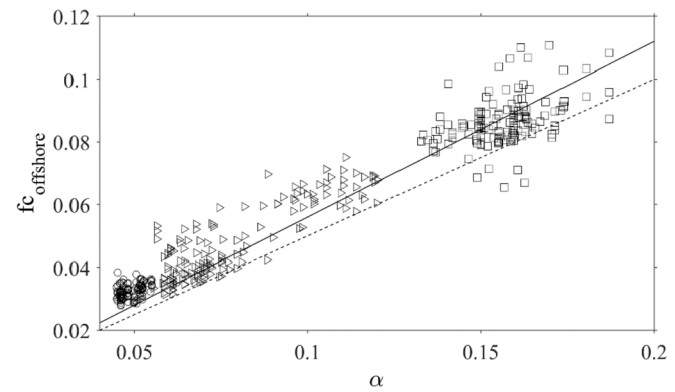


Fig. 3. Hourly cut-off frequency from offshore wave measurements ($fc_{offshore}$) at Grand Popo (squares), Nha Trang (triangles) and Mataquito (circles) as a function of swash slope α . Solid line stands for linear best fit ($fc_{offshore} = 0.56\alpha$, $r^2 = 0.71$, significant at 95% level) while dashed line is $fc_{offshore} = 0.5\alpha$.

3.2. Profile reconstruction from swash-based reflection

The link between α and fc is used here to invert the intertidal beach profile from offshore estimates of fc at different beaches and tidal levels. The vertical resolution of the method depends on the ADCP sampling frequency (hourly here) and the tidal range, thus the vertical resolution is no larger than ~0.25 m at mid tide for these micro-tidal sites. The horizontal resolution depends on the swash slope. The profile is reconstructed by integrating the swash slope estimates over a full tidal cycle. Fig. 4 shows the application of the method to daily beach profile reconstruction at the three sites. Note that the new method provides only the swash slope and not the horizontal location of this slope, thus

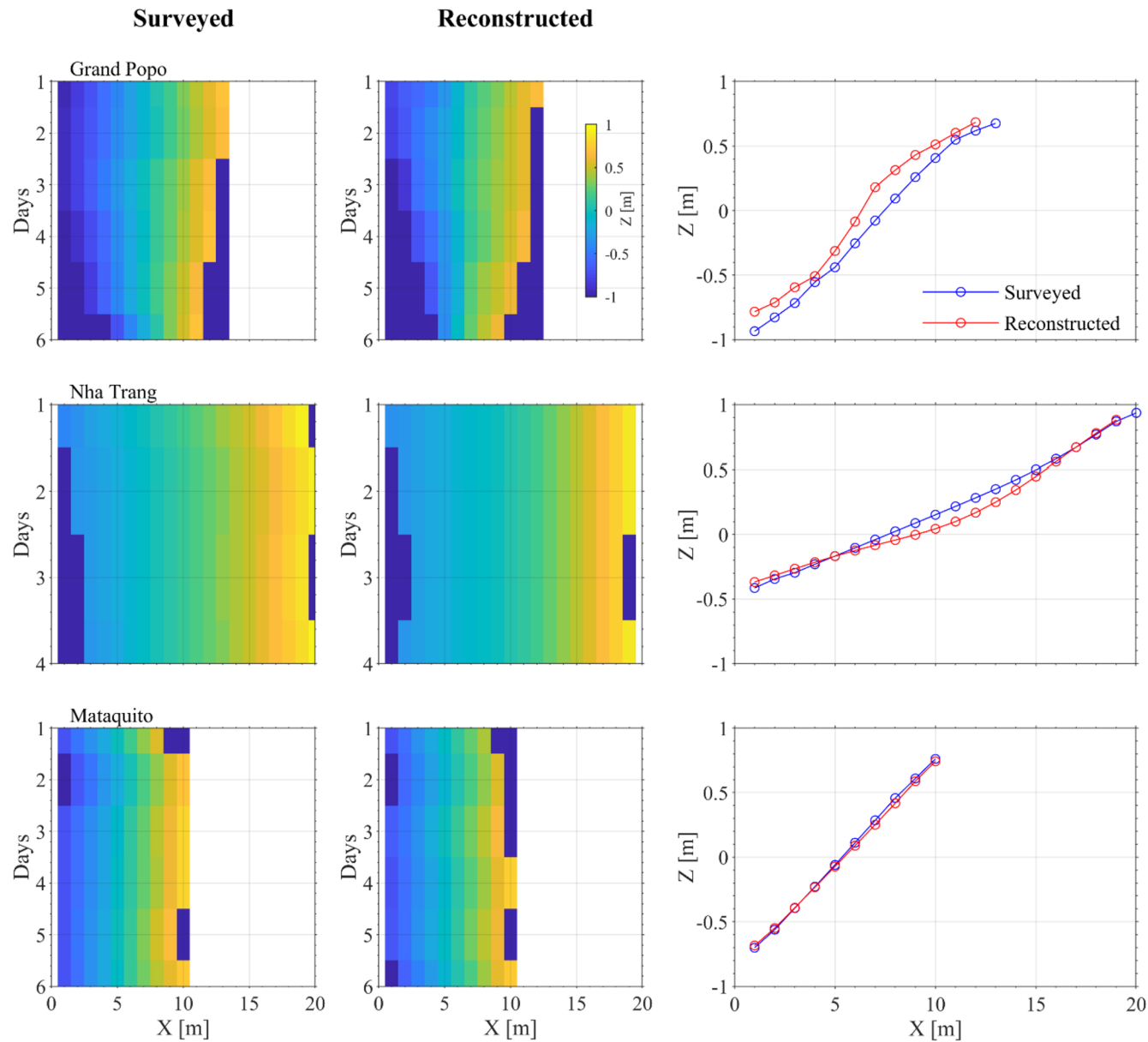


Fig. 4. Intertidal beach profile. The daily surveyed profiles are shown in the first column and those estimated from the offshore ADCP in the second column. In the third column are shown the averaged profiles over the duration of the experiments of surveyed and estimated profiles. The reconstructed profile horizontal origin is set according to the survey data. The circles in the right panels indicate the center of each of the incremental sections of the profile.

the position of the profile toe has to be provided. A global translation of the profile could not be detected with this equilibrium method which captures the shape changes of the intertidal profile. Nevertheless, the profile estimates show a good overall agreement with the surveys for the three sites, and the new method is able to capture the observed breaks in slope. RMS errors on the daily profiles are 0.15, 0.06 and 0.04 m respectively for Grand Popo, Nha Trang and Mataquito with the error increasing with the beach slope. Noteworthy, the relatively large error observed at Grand Popo might also be attributed to the presence of a cuspatate pattern (Senechal et al., 2014, 2015; Almar et al., 2018b) as well as the steep, reflective nature of the beach. The resulting small-scale (~ 30 m) alongshore irregularities in the swash are not captured by the method and are smoothed out at the location of wave measurements. Because of this, the alongshore resolution of the method depends on the distance to the shore and the method is expected to always perform better at alongshore-uniform beaches.

4. Conclusions

The reconstruction of the intertidal beach profile from reflected waves was tested using three field datasets covering a wide range of hydro-morphological conditions: dissipative (Mataquito beach), intermediate (Nha Trang beach), and reflective (Grand Popo beach). The swash was found to behave as a low-pass filter on reflected waves, with a cut-off frequency that primarily depends on swash slope. Despite the multiple sources of scatter, reasonable agreement was found between video-derived swash spectrum saturation tail and the shortest reflected waves, computed from deep water directional wave measurements. The potential to estimate these parameters remotely makes an estimation of the swash slope possible from offshore wave measurements. By integrating this swash slope over a tidal cycle, the intertidal beach profile can be reconstructed. Although the method is able to capture changes in the shape of the profile, it may not be possible to monitor the change in volume related to a cross-shore displacement of the profile (either accretion or erosion) that would be interpreted as “no change”. Our

results clearly show the potential of this method to estimate complex intertidal beach profile with RMS errors smaller than 0.15 m. In our dataset, the error increases with the beach slope; bigger errors are expected for steeper slopes. The results presented in this paper demonstrate the potential of this new method, however it is recommended that the approach be tested at further sites with longer timeseries to better confirm the general applicability.

Acknowledgments

Mataquito exp. supported by Chilean grants Conicyt/Fondecyt/1120878 and Conicyt/Fondap/15110017, Grand Popo exp. by French INSU/CNRS EC2CO-LEFE/IRD, UNESCO co-chair ICPMA/IRHOB, and Nha Trang exp. by Vietnamese MOST (BKHCN/NDT-HD/2013/110 and NDT.24.FRA.16). We are greatly indebted to the naval services of Benin at Grand Popo for their logistic support during the field experiment and for allowing the installation of the permanent video system on the se-maphore. E.B.' work was supported through CNES' post-doctoral fellowship program (CNES - Centre National d'Etudes Spatiales). P.A.C. was also supported by Chilean grants Conicyt/PIA/FB0821 and Conicyt/Fondecyt/1170415. C.B. was funded by the Engineering and Physical Sciences Research Council project "WAVes in Shallow water" (WASH) (EP/N019237/1). This research has received support from French grants through ANR (COASTVAR: ANR-14-ASTR-0019).

References

- Aarninkhof, Stefan G.J., Turner, Ian L., Dronkers, Thomas DT., Caljouw, Mark, Nipius, Leann, 2003. A video-based technique for mapping intertidal beach bathymetry. *Coast. Eng.* 49 (4), 275–289.
- Almar, R., Ranasinghe, R., Senechal, N., Bonneton, P., Roelvink, D., Bryan, K., Marieu, V., Parisot, J.P., 2012. Video based detection of shorelines at complex meso-macrotidal beaches. *J. Coastal Res. COAS* 28 (5), 1040–1048 49646.
- Almar, R., Catalan, P., Ibáñez, R., Blenkinsopp, C., Cienfuegos, R., Villagrán, M., Aguilera, J.-C., Castelle, B., 2014a. Comparison of swash zone measurements during energetic wave conditions at a dissipative beach. In: International Conference on Coastal Engineering, Seoul, Korea, June 2014, pp. 1–8.
- Almar, R., Du Penhoat, Y., Honkonou, N., Castelle, B., Laibi, R., Anthony, E., Senechal, N., Degbe, G., Chuchla, R., Sohou, Z., Dorel, M., 2014b. The Grand Popo experiment, Benin. *J. Coastal Res. SI* 70, 651–656 ISSN 0749-020.
- Almar, R., Michallet, H., Cienfuegos, R., Bonneton, P., Tissier, M.F.S., Ruessink, B.G., 2014c. On the use of the radon transform in studying nearshore wave dynamics. *Coast. Eng.* 92, 24–30.
- Almar, R., Blenkinsopp, C., Almeida, L.P., Cienfuegos, R., Catalan, P., 2017. Wave runup video motion detection using the Radon Transform. *Coast. Eng.* 130, 46–51.
- Almar, R., Blenkinsopp, C., Almeida, L.P., Cienfuegos, R., Catalan, P., Viet, N.T., 2018a. A new remote predictor of wave reflection based on runup asymmetry. *Estuarine, Coastal and Shelf Science* 217, 1–8.
- Almar, R., Nicolae Lerma, A., Castelle, B., Scott, T., 2018b. On the influence of reflection over a rhythmic swash zone on surf zone dynamics. *Ocean Dynam.* 68 (6). <https://doi.org/10.1007/s10236-018-1165-5>.
- Andriolo, U., Almeida, L.P., Almar, R., 2018. Coupling terrestrial LiDAR and video imagery to perform 3D intertidal beach topography. *Coast. Eng.* 140, 232–239.
- Anthony, E., 1998. Sediment-wave parametric characterization of beaches. *J. Coast. Res.* 14 (1), 347–352.
- Baldock, T., Holmes, P., 1999. Simulation and prediction of swash oscillations on a steep beach. *Coast. Eng.* 36, 219–242.
- Baquerizo, A., Losada, J.M., Smith, M.A., Kobayashi, N., 1997. Cross-shore variation of wave reflection from beaches. *J. Waterway, Port, Coastal Ocean Eng. ASCE* 123, 274–279.
- Battjes, J., 1974. Surf similarity. In: 14th Coastal Engineering Conference. Am. Soc. Of Civ. Eng., Copenhagen, Denmark, pp. 466–480.
- Bernabeau, A.M., Medina, R., Vidal, C., 2003. Wave reflection on natural beaches: an equilibrium beach profile model. *Estuar. Coast Shelf Sci.* 57, 577–585.
- Bertin, X., De Bakker, A., Van Dongeren, A., Coco, G., André, G., et al., 2018. Infragravity waves: from driving mechanisms to impacts. In: Earth-Science Reviews, vol. 177. Elsevier, pp. 774–799.
- Blenkinsopp, C., Mole, M.E., Turner, I.L., Peirson, W.L., 2010. Measurements of the time-varying profile across the swash zone using an industrial LiDAR. *Coast. Eng.* 57, 1059–1106.
- Bowen, A., 1977. A universal form for shoreline run-up spectra? *J. Geophys. Res.* 82, 2577–2581.
- Broccolini, M., Baldock, T., 2008. Recent advances in modeling swash zone dynamics: influences of surf-swash interaction on nearshore hydrodynamics and morphodynamics. *Rev. Geophys.* 46 (3), RG3003.
- Cienfuegos, R., Villagrán, M., Aguilera, J.-C., Catalan, P., Castelle, B., Almar, R., 2014. Video monitoring and field measurements of a rapidly evolving coastal system: the river mouth and sand spit of the Mataquito river in Chile. *J. Coast. Res.* 70, 639–644 SI.
- Davies, A.G., 1982. The reflection of water-wave energy by undulations on the seabed. *Dyn. Atmos. Oceans* 6, 207–232.
- de Bakker, A., Tissier, M., Ruessink, B., 2014. Shoreline dissipation of infragravity waves. *Cont. Shelf Res.* 72 (1), 73–82.
- Díaz-Sánchez, R., López-Gutiérrez, J.S., Lechuga, A., Negro, V., Esteban, M.D., 2013. Direct estimation wave setup as a medium level in swash. In: Conley, D.C., Masselink, G., Russell, P.E., O'Hare, T.J. (Eds.), Proceedings 12th International Coastal Symposium (Plymouth, England), Journal of Coastal Research, Special Issue, vol. 65. pp. 201–206.
- Didier, D., Bernatchez, P., Augereau, E., Caulet, C., Dumont, D., Bismuth, E., Cormier, L., Floc'h, F., Delacourt, C., 2017. LiDAR validation of a video-derived beachface topography on a tidal flat. *Rem. Sens.* 9 (8), 826.
- Elgar, S., Herbers, T., Guza, R., 1994. Reflection of ocean surface gravity waves from a natural beach. *J. Phys. Oceanogr.* 24 (7), 1503–1511.
- Elgar, S., Raubenheimer, B., Herbers, T.H.C., 2003. Bragg reflection of ocean waves from sandbars. *Geophys. Res. Lett.* 30, 1016. <https://doi.org/10.1029/2002GL016351>.
- Guedes, R., Bryan, K., Coco, G., Holman, R., 2011. The effects of tides on swash statistics on an intermediate beach. *J. Geophys. Res.* 116, C04008.
- Guedes, R., Bryan, K., Coco, G., 2013. Observations of wave energy fluxes and swash motions on a low-sloping, dissipative beach. *J. Geophys. Res.* 118 (7), 1–19.
- Guza, R., Thornton, E., 1982. Swash oscillations on a natural beach. *J. Geophys. Res.* 87, 483–491.
- Heikkilä, J., Silven, O., 1997. A four-step camera calibration procedure with implicit image correction. *Computer Vision and Pattern Recognition*. In: Proceedings of the IEEE Computer Society Conference, pp. 1106–1112.
- Holland, K.T., Holman, R.A., 1993. The statistical distribution of swash maxima on natural beaches. *J. Geophys. Res.* 98 (C6), 10271–10278.
- Holland, K., Puleo, J., Kooney, T., 2001. Quantification of swash flows using video-based particle image velocimetry. *Coast. Eng.* 44 (2), 6577.
- Holland, K., Holman, R., Lippmann, T., Stanley, J., Plant, N., 2013. Practical use of video imagery in nearshore oceanographic field studies. *Ocean Eng.* 22 (1), 81–82.
- Hughes, S., Fowler, J., 1995. Estimating wave-induced kinematics at sloping structures. *J. Waterw. Port, Coast. Ocean Eng.* 121 (4), 209–215.
- Hughes, S., Mosley, A., 2007. Hydrokinematic regions within the swash zone. *Cont. Shelf Res.* 27 (15), 2000–2013.
- Hughes, M.G., Aagaard, T., Baldock, T.E., Power, H.E., 2014. Spectral signatures for swash on reflective, intermediate and dissipative beaches. *Mar. Geol.* 355, 88–97.
- Huntley, D., Guza, R., Bowen, A., 1977. A universal form for shoreline run-up spectra? *J. Geophys. Res.* 82, 2577–2581.
- Iribarren, C., Nogales, C., 1949. Protection des ports. In: XVIIth International Navigation Congress, Section II, Communication, pp. 31–80.
- Laibi, R., Anthony, E., Almar, R., Castelle, B., Senechal, N., 2014. Morphodynamic characterisation of the human-impacted Bight of Benin sand barrier coast, West Africa. *J. Coast. Res.* 70, 079–083 ISSN 0749-0208.
- Lefebvre, J.-P., Almar, R., Viet, N., Uu, D., Thuan, D., Binh, L., Ibáñez, R., Duc, N., 2014. Contribution of swash processes generated by low energy wind waves in the recovery of a beach impacted by extreme events: Nha Trang, Vietnam. *J. Coastal Res. SI* 70, 663–668.
- Ludka, B.C., Guza, R.T., O'Reilly, W.C., Yates, M.L., 2015. Field evidence of beach profile evolution toward equilibrium. *J. Geophys. Res., Oceans* 120 (11), 7574–7597.
- Mei, C.C., 1985. Resonant reflection of surface waves by periodic sand bars. *J. Fluid Mech.* 152, 315–335.
- Miche, R., 1951. Le pouvoir réfléchissant des ouvrages maritimes exposés à l'action de la houle. *Ann. Ponts Chaussées* 121, 285–319.
- Miles, J., Russell, P., 2004. Dynamics of a reflective beach with a low tide terrace. In: Continental Shelf Research COAST3D Special Issue, vol. 24. pp. 1219–1247.
- Mizuguchi, M., 1984. Swash on a natural beach. *Coastal Engineering Proceedings* 19 2156–1028.
- Phillips, M.S., Blenkinsopp, C.E., Splinter, K., Harley, M.D., Turner, I.L., 2019. Modes of berm and beachface recovery following storm reset: observations using a continuously scanning lidar. *J. Geophys. Res.: Earth Surface*. <https://doi.org/10.1029/2018JF004895>.
- Raubenheimer, B., Guza, R.T., Elgar, S., 1996. Wave transformation across the inner surf zone. *J. Geophys. Res.* 101, 25589–25597.
- Ruessink, B., Kleinhans, M., Van den Beukel, P., 1998. Observations of swash under highly dissipative conditions. *J. Geophys. Res.* 103, 3111–3118.
- Ruggiero, P., Holman, R., 2004. Wave run-up on a high-energy dissipative beach. *J. Geophys. Res.* C06025.
- Sallenger, A., Holman, R., 1985. Wave energy saturation on a natural beach of variable slope. *J. Geophys. Res.* 90-C6/11, 939–944.
- Senechal, N., Coco, G., Bryan, K., Holman, R., 2011. Wave runup during extreme storm conditions. *Journal of Geophysical Research - Oceans* 116, C07032.
- Senechal, N., Laibi, R., Almar, R., Castelle, B., Degbe, G., DuPenhoat, Y., Chuchla, R., Honkonou, N., 2014. Beach cusp dynamics on a reflective beach. *J. Coast. Res.* 70, 669–674 ISSN 0749-0208.
- Senechal, N., Castelle, B., Biausque, M., Floc'h, F., Scott, T., Almar, R., Anthony, E.J., Du Penhoat, Y., 2015. Beach Cusp Destruction Sequences Observed under Erosion and Accretion Conditions, vol. 2015 Coastal Sediment, San Diego, USA.
- Sheremet, A., Guza, R.T., Elgar, S., Herbers, T.H.C., 2002. Observations of nearshore infragravity waves: seaward and shoreward propagating components. *J. Geophys. Res.* 107. <https://doi.org/10.1029/2001JC000970.C8>.
- Suhayda, J., 1974. Standing waves on beaches. *J. Geophys. Res.* 79 (21), 3065–3071.
- Sutherland, J., O'Donoghue, T., 1998. Characteristics of wave reflection spectra. *J. Waterw. Port, Coast. Ocean Eng.* 124 (6), 303–311.

- Taira, K., Nagata, Y., 1968. Experimental study of wave reflection by a sloping beach. *J. Oceanogr. Soc. Jpn.* 24 (5), 242–252.
- Van Dongeren, A.R., Battjes, J., Janssen, T., Van Noorloos, J., Steenhauer, K., Steenbergen, G., Reniers, A., 2007. Shoaling and shoreline dissipation of low-frequency waves. *J. Geophys. Res.* 112, C02011.
- Vousdoukas, M.I., 2014. Observations of wave run-up and groundwater seepage line motions on a reflective-to-intermediate, meso-tidal beach. *Mar. Geol.* 350. <https://doi.org/10.1016/j.margeo.2014.02.005>.
- Yu, J., Mei, C.C., 2000. Formation of sand bars under surface waves. *J. Fluid Mech.* 416, 315–348.